Effects of aging heat treatment on microstructure and corrosion behavior of friction surfacing treated Al−Zn−Mg−Cu matrix composite

Hamed JAMSHIDI AVAL

Department of Materials Engineering, Babol Noshirvani University of Technology,
Shariati Avenue 47148-71167, Babol, Iran

Abstract: The effect of artificial aging heat treatment on the microstructure and corrosion behavior of Al−Zn−Mg−Cu matrix composite was studied. Nickel-aluminide reinforcement was fabricated in-situ during the stir casting process of Al−Zn−Mg−Cu alloy. After friction surfacing of the consumable rod of an as-cast composite on AA1050 substrate and post-processing artificial aging heat treatment at 125 °C for 18 h, significant grain growth was observed in the nickel-free sample. Moreover, the presence of nickel-aluminide reinforcement in the microstructure of composite resulted in the formation of bimodal microstructure. The presence of nickel-rich particles and the strengthening mechanism through precipitates could help increase the hardness and strength in the nickel-containing sample. After artificial aging heat treatment, the shear strength and hardness of composite containing nickel-aluminide increased by 24% and 13%, respectively, more than those of the aluminum matrix. Before aging heat treatment, the pitting corrosion resistance was significantly improved by the presence of nickel-containing particles. After aging heat treatment due to the adsorption of more significant amount of soluble copper by nickel-rich particles in the nickel-containing sample, corrosion resistance decreased by 39% compared to that of the nickel-free sample.
Key words: aluminum matrix composite; nickel-aluminide reinforcement; friction surfacing; artificial aging heat treatment; corrosion behavior

1 Introduction

According to the needs of the industry, the engineering materials must be designed most efficiently with the longest permanence. Prolonging the durability of materials is incredibly possible by improving their surface properties. Surface engineering in the two branches of surface processing and coating increases the durability of materials. In the surface processing methods, the properties are improved by polishing or modifying the surface [1,2]; however, in coating methods, a secondary material is coated on the surface of the material. The coating methods include fusion base and solid-state methods [3−6]. Due to the disadvantages and limitations of fusion-based methods, such as performing the process at high temperatures, attention has been drawn to solid-state methods.

The materials selected as a suitable option for coating are composite materials. In recent years, aluminum matrix composites (AMCs) have received considerable attention due to their lightweight, low thermal expansion coefficient, good machining, low cost, and good thermal conductivity. Although composites with ceramic reinforcing particles have high strength and sufficiently high corrosion and wear resistance, their toughness is low. Hard metal particles can be used as reinforcements in the aluminum matrix as an alternative method to maintain the ductility of

the composite. However, it is challenging to retain metal particles as reinforcements. Metals with low solubilities, such as nickel, iron, and titanium react efficiently with aluminum by forming aluminide with rapid kinetics.

The addition of nickel to aluminum alloys effectively increases the strength at room temperature and higher temperatures [7−10]. This phenomenon has been reported in various alloys, including Al−Si, Al−Mg−Si−Mn, Al−Si−Cu−Mg, and Al−Zn−Mg−Cu. AKOPYAN et al [11] studied the phase diagram of Al−Zn−Mg−(Cu)−Ni alloy using Thermal-Calo software and observed that eutectic nickel forms Al−Al$_3$Ni in structure. The presence of nickel in aluminum alloys through the formation of nickel-aluminide composition due to high elastic modulus (116−152 GPa), high hardness (5130 MPa), as well as high strength (2160 MPa) leads to the strengthening of aluminum alloys [10]. Limited studies have been conducted on AA7xxx series aluminum alloy matrix composite by various researchers using ceramic and metal reinforcing particles. Using the stir casting process, SURESH et al [12] produced the Mg/Al$_2$O$_3$/AA7075 composite. The average particle size of Al$_2$O$_3$ was 20−30 nm, and the content of Al$_2$O$_3$ reinforcing particles in this study was 1, 2, 3, and 4 wt.%. They found that adding 1 wt.% of micro-magnesium powder improved the wettability of Al$_2$O$_3$ reinforcing particles. The results showed that the T6 heat treatment on Mg/Al$_2$O$_3$/AA7075 composite improves mechanical properties. Furthermore, by increasing the mass fraction of Al$_2$O$_3$ particles, the hardness, tensile strength, and toughness of the composite were improved compared to AA7075-based alloy. KHAKI-DAVOUDI et al [13] investigated the effect of adding nickel to the AA7075 aluminum matrix composite using a semi-solid casting method. The results showed that with increasing the content of nickel to 5 wt.%, a decrease in strength, toughness, elongation, and hardness was observed. This reduction in mechanical properties is due to the agglomeration of particles in the matrix and the high percent of porosity. Moreover, increasing the stirring temperature causes a proper distribution of particles in the matrix, and a better reaction is established between the particles and the matrix. SALARIEH et al [14] investigated the effect of adding titanium reinforcement to AA7075 aluminum alloy. The results showed that the ultimate tensile strength, elongation, and toughness of the composite increased by 12%, 0.84%, and 9%, respectively, compared to those of the matrix.

Al−Zn−Mg−Cu alloys are among precipitation-hardenable aluminum alloys. According to Refs. [15,16], adding nickel to aluminum alloys can absorb copper in the aluminum matrix and reduce the amount of copper dissolved in the matrix. Therefore, it can be expected that the precipitation sequence of the alloy will be affected. Consequently, in the present study, the effect of nickel addition on the microstructure and corrosion behavior of Al−Zn−Mg−Cu matrix composite reinforced with nickel-aluminide particles after heat treatment were investigated.

2 Experimental

In the present study, Al−Zn−Mg−Cu alloy with a chemical composition of 0.03% Si, 0.03% Fe, 1.63% Cu, 6.61% Zn, 3.12% Mg, 0.18% Cr, and Al balance (all in wt.%) as a composite matrix has been used. Nickel powder with particle size of 20−100 μm and purity of 99% has also been used as an additive. Aluminum alloy with a chemical composition of 0.07% Si, 0.28% Fe, 0.05% Cu, 0.01% Mg, 0.02% Mn, and Al balance (in wt.%) and dimensions of 10 cm × 10 cm was used as a substrate. The semi-solid casting method was used to create the composite. In the compocasting process, the stirring temperature of 630 °C, stirring speed of 450 r/min, stirring time of 10 min, and 3 wt.% nickel powder were used. Details of composite fabrication were described in Ref. [13]. After casting, the consumable rod was homogenized at 550 °C for 12 h. Then, the cast rods were machined to construct consumable rods with a diameter and a length of 20 and 100 mm, respectively. Based on initial tests and cladding operations using a rotational speed of 400− 1200 r/min, a traverse speed of 75−125 mm/min, and an axial feeding rate of 100−200 mm/min, the highest cladding efficiency was obtained using a rotational speed of 800 r/min, a traverse speed of 100 mm/min and an axial feeding rate of 125 mm/min. Therefore, all cladding operations were performed using the parameters mentioned above.

After cladding operations, the metallographic and corrosion samples were extracted from the composite based on Fig. 1. After grinding and

polishing metallographic samples to detect grain boundaries, the metallographic samples were etched using Keller etchant solution with a chemical composition of 95 mL distilled water, 1.5 mL HCl, 1 mL HF, and 2.5 mL HNO$_3$. The microstructure was examined using an NGF−120A optical microscope and an FEI SEM QUANTA 200 electron microscope equipped with an EDS detector. The mechanical properties of the composite were evaluated using a micro-hardness test. The micro-hardness test was performed by utilizing a KOOPA-UV1 universal hardness tester by applying a load of 0.98 N (100 g) for 10 s. After solid-solution treatment at 480 °C for 2 h, artificial aging heat treatment was performed at 125 °C for 18 h to investigate the effect of heat treatment on the microstructure, mechanical properties, and composite corrosion. Electrochemical experiments were performed by drawing polarization curves to evaluate the corrosion resistance of the composite.

All investigations were conducted using the electrochemical workstation CS350. During the polarization experiments, a scanning rate of 1 mV/s was utilized to polarize the specimens at 250 mV below open circuit potential. Also, the saturated calomel electrode (SCE) was used as the reference electrode.

3 Results and discussion

Figure 2 shows the cross-section of two samples with and without nickel. Applying a composite with a nickel-containing rod has reduced the dimensions of the composite compared to a nickel-free sample. As shown in Fig. 2, the enclosed area between the effective width and the effective thickness of the composite in the sample containing nickel and without nickel is 32.4 and 49.3 mm^2, respectively. Although the applied composite layer has a sound interface in both samples, the reduction
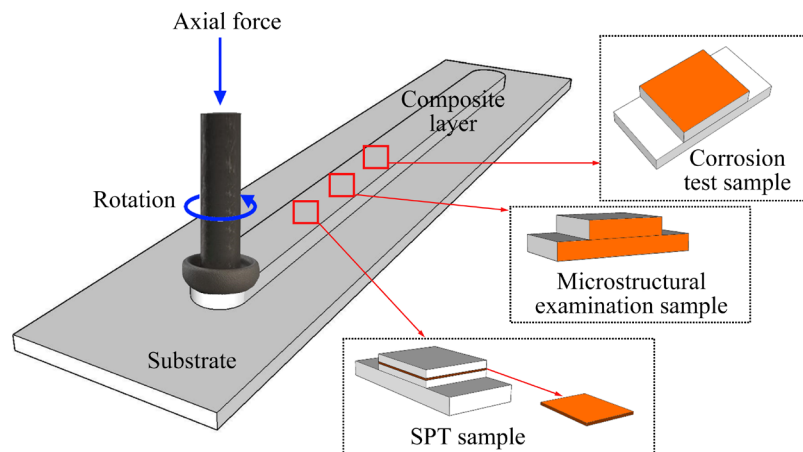

Fig. 1 Schematic illustration of extraction position of microstructural examination, SPT test, and corrosion examination samples (The highlighted area shows the position of the examination)
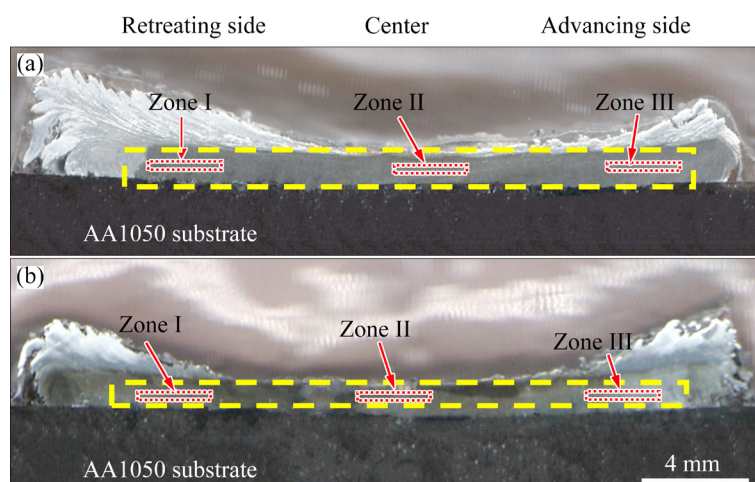

Fig. 2 Cross-section of samples: (a) Nickel-free; (b) Nickel-containing

of the composite dimensions in the nickel-containing sample is due to the difference in the plastic deformation behavior of the two consumable rods during the cladding process. Due to the lower yield strength of the consumable rod without nickel (104.23 MPa) than the yield strength of the consumable rod containing nickel (121.16 MPa), it can be expected that the consumable rod without nickel, due to its higher deformation capability, deforms easily and leads to a composite with greater width and thickness, and ultimately greater

cladding efficiency.

In Fig. 3, the optical microscope images of different areas of nickel-containing and nickel-free samples are shown. Although there is a noticeable difference in the grain size of the two composites, there is no noticeable difference in the grain size of the advancing side, retreating side, and center of the sample, regardless of a nickel is applied. Measurement of grain size of nickel-containing composite showed that the average grain size of the advancing side, retreating side, and center of the
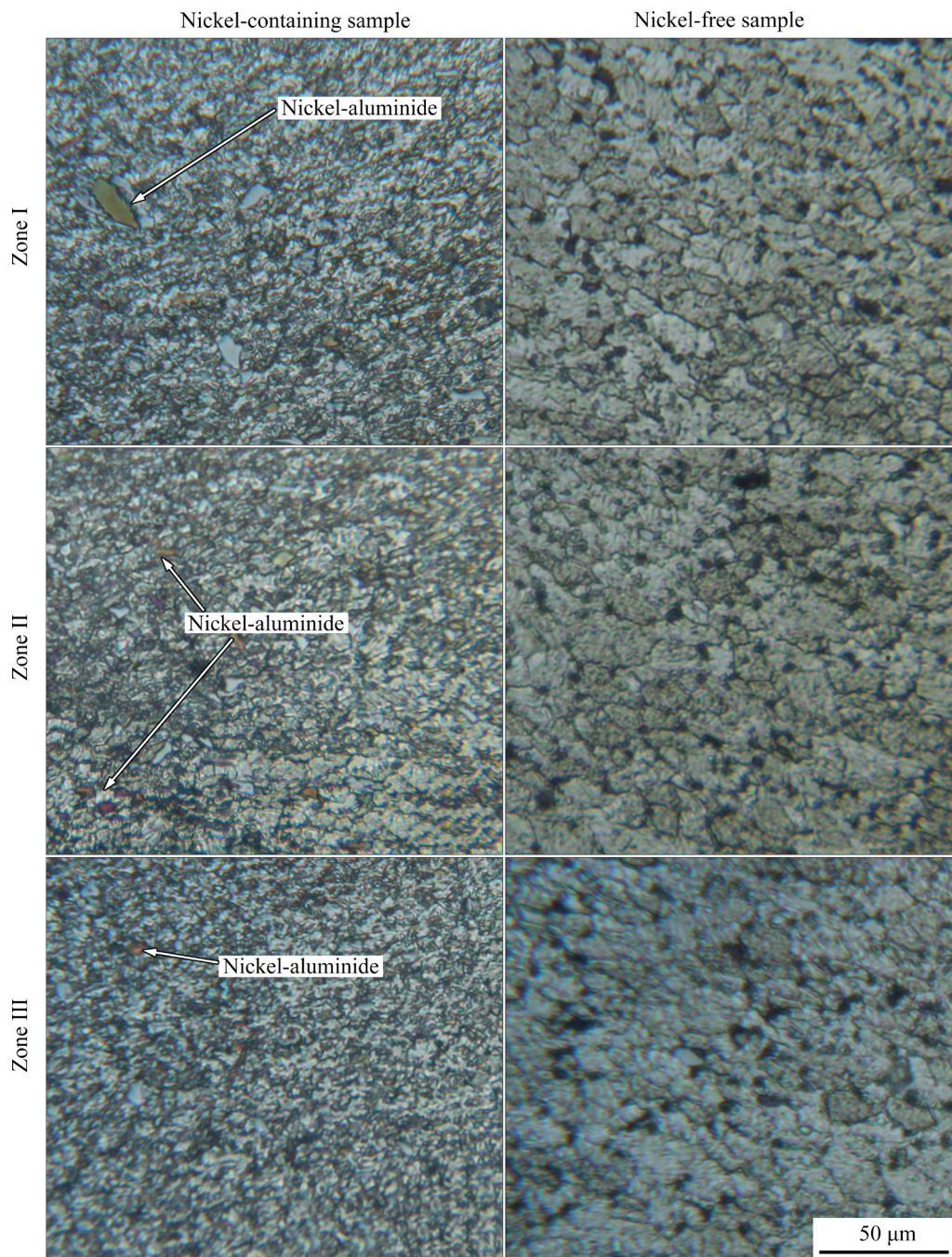

Fig. 3 Optical microscope images of different areas of nickel-containing and nickel-free samples

sample is (2.1±0.9), (2.9±0.6) and (2.4±0.8) μm, respectively, and in the sample without nickel, the average grain size of advancing side, retreating side and center of the sample is (5.2±0.5), (5.9±0.3) and (5.3±0.5) μm, respectively. The coarser grains in the nickel-free sample can be traced to two factors. Firstly, the lower temperature during the process in the nickel-containing sample allows for less grain growth. Secondly, the nickel-rich particles act as barriers to the movement of dislocation and grain boundaries and inhibit grain growth. However, higher temperatures during cladding and the absence of nickel-rich secondary phase particles in the nickel-free sample can lead to the grain growth and coarser grain size in the nickel-free sample.

Figure 4 shows the microstructure of the center zone of samples (Zone II) after the aging heat treatment. As is evident, significant grain growth is observed in the nickel-free sample due to the dissolution of reinforcing precipitates during solid-solution treatment and the absence of secondary phase particles that can inhibit grain growth in this sample. Therefore, significant grain growth in the nickel-free sample is not unexpected. Although grain growth is visible in the sample containing nickel, the growth of grain is much lower than that of the sample without nickel. As is observed, another critical point is the formation of bimodal microstructure in the sample containing nickel after heat treatment. The formation of this type of microstructure is probably due to the presence of nickel-rich particles. In this way, in areas where these particles are less dense, the grains grow easily; however, in areas with a higher density of these particles, there is not enough growth opportunity for grains, so the difference in grain boundary motion ability in different areas can lead to the formation of bimodal microstructure.

The microstructure of the center of the composites has been studied using SEM to investigate the microstructural changes in different samples, and the results are reported in Fig. 5. According to EDS analysis in nickel-free samples, precipitates and secondary phase particles are S-Al$_2$CuMg, Fe-rich particles, and MgZn$_2$. However, in the sample containing nickel, in addition to the mentioned precipitates and secondary phase particles, Ni−Cu-rich particles (i.e., Al$_3$NiCu particles) are also visible. As is evident, after the

aging heat treatment, the size of the precipitates is smaller. Another essential point to note in the images is the smaller amount of S-Al$_2$CuMg precipitates in samples containing nickel. The presence of nickel-rich particles causes the adsorption of copper in the aluminum matrix [16], leading to a reduction of copper in the aluminum matrix. After solid solution and aging heat treatment of sample containing nickel, due to providing more opportunity to absorb copper in the aluminum matrix, the copper amount available for
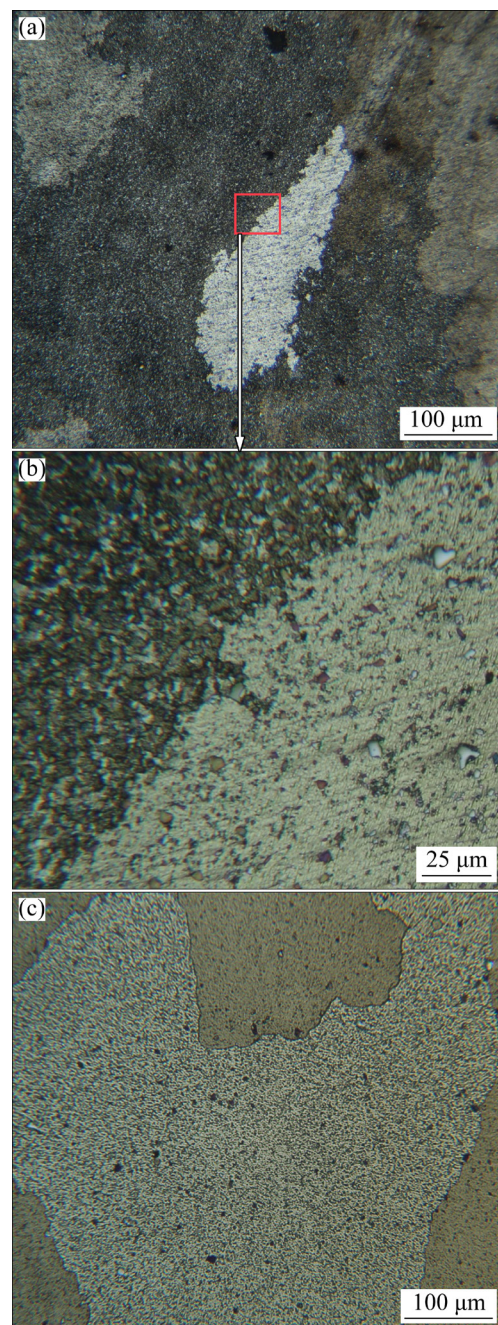

Fig. 4 Microstructure of center zone of samples after artificial aging heat treatment: (a, b) Nickel-containing; (c) Nickel-free
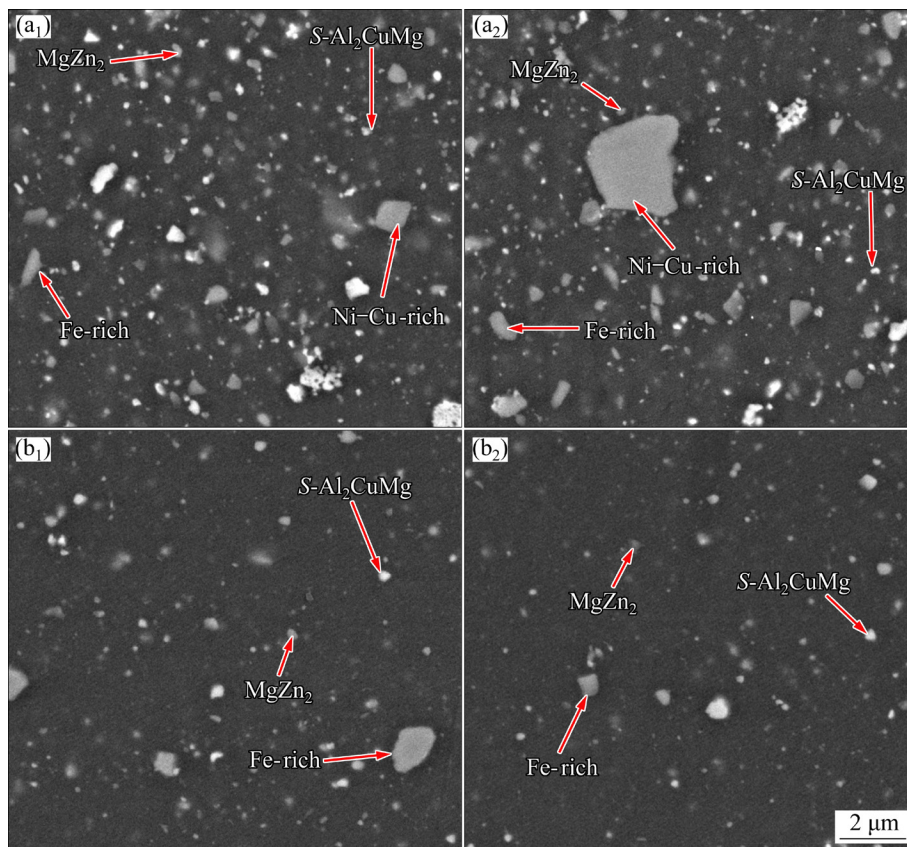
Fig. 5 SEM images of precipitates and second phase particles of samples before (a$_1$, b$_1$) and after (a$_2$, b$_2$) aging: (a$_1$, a$_2$) Nickel-containing; (b$_1$, b$_2$) Nickel-free

precipitation of S-Al$_2$CuMg precipitates decreases, and the possibility of S precipitates during aging decreases. Finally, lower amount of S precipitates form in the sample containing nickel after aging.

The average hardness and shear strength of different samples are reported in Fig. 6. As is observed, after aging heat treatment, the hardness and shear strength of both nickel-containing and nickel-free samples have increased. Given that the amount of S-Al$_2$CuMg precipitates in the nickel-containing sample decreased after heat treatment, it may be expected that the hardness and strength of the sample should be reduced after heat treatment. However, in justifying the trend of changes in hardness and strength in two samples containing nickel and without nickel, the effect of different strengthening factors should be examined. According to different sources [17−19], the strengthening mechanisms such as strengthening through a solid solution, strengthening through precipitates and secondary phase particles, strengthening through grain boundary, and modulus strengthening mechanism can affect the variation in
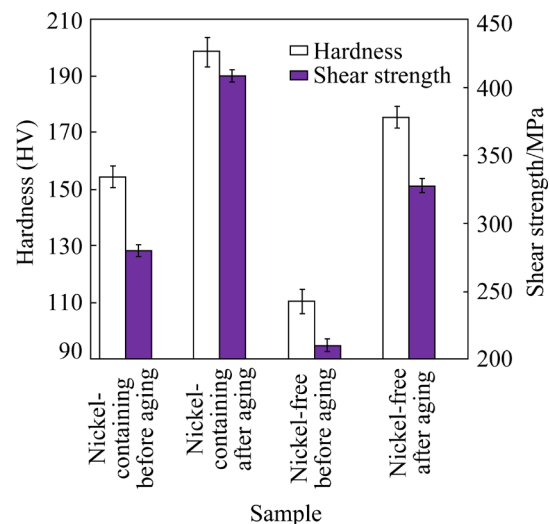

Fig. 6 Average hardness and shear strength of different samples

hardness and strength of different samples. Based on EDS analysis, the content of copper and zinc in the aluminum matrix in the composite containing nickel before and after aging heat treatment is 0.38 at.% Cu, 0.44 at.% Zn and 0.12 at.% Cu, 0.22 at.% Zn, respectively. Furthermore, the content

of copper and zinc in the aluminum matrix in the sample without nickel before and after aging heat treatment is 0.29 at.% Cu, 0.84 at.% Zn and 0.18 at.% Cu, 0.59 at.% Zn, respectively. Due to the small amount of soluble elements in the aluminum matrix, it can be expected that the effect of the strengthening mechanism through the solid solution in the composites containing nickel and free one is negligible. However, fewer S-Al$_2$CuMg precipitates in the nickel-containing sample can adversely affect the mechanical properties of the composite. However, since the hardening in Al−Zn−Mg−Cu alloys occurs mainly through η-MgZn$_2$ precipitates [20,21], it can be expected that the lack of significant differences in the amount of η-MgZn$_2$ precipitates in the two nickel-containing and nickel-free samples means that the strengthening mechanism through precipitates will not differ much between the two samples. Smaller grain size and higher density of grain boundaries in nickel-containing samples before and after heat treatment can help increase the mechanical properties of nickel-containing sample compared to nickel-free sample. Another noteworthy point is the formation of nickel-aluminide compounds in the sample containing nickel, which, according to Refs. [10,22], will positively affect strengthening. There is a significant difference in the elastic modulus of nickel aluminide compounds and the aluminum matrix. This difference in elastic modulus can cause a significant difference in shear modulus. Under these conditions, during the movement of the dislocations, at the vicinity of nickel-aluminide particles, a strong interaction will be created between the dislocation and the stress field around the particles, which helps strengthen the composite. Consequently, the higher strength and hardness in the sample containing nickel before heat treatment than those of the sample free of nickel are due to the predominance of strengthening mechanisms through the grain boundary and the modulus strengthening mechanism. After aging heat treatment, although significant grain growth is observed in the two samples, the presence of nickel-rich particles and the strengthening mechanism through precipitates can help increase the hardness and strength in the nickel-containing sample.

The polarization curves of different samples are shown in Fig. 7 to investigate the effect of

microstructure and heat treatment on corrosion behavior. Also, Figs. 8 and 9 show the Nyquist diagram and Bode plots of different samples, respectively. The electrochemical parameters obtained from the polarization measurements are summarized in Table 1. Concentration-controlled cathodic polarization curves were depicted from the curves below corrosion potential (φ_{corr}). In the nickel-free sample, the corrosion potential of
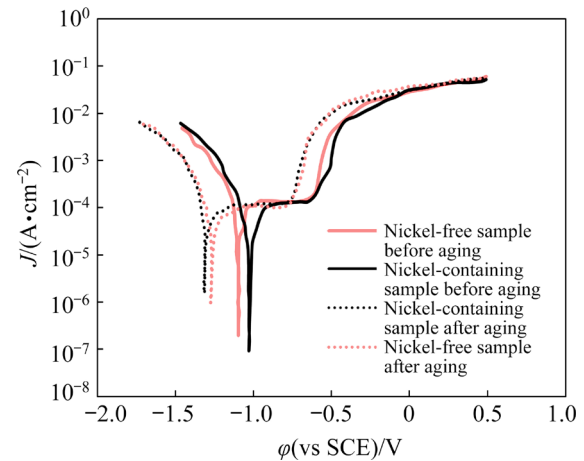

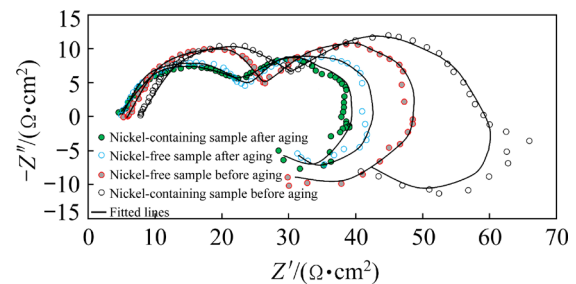**Fig. 7** Polarization curves of nickel-containing and nickel-free samples

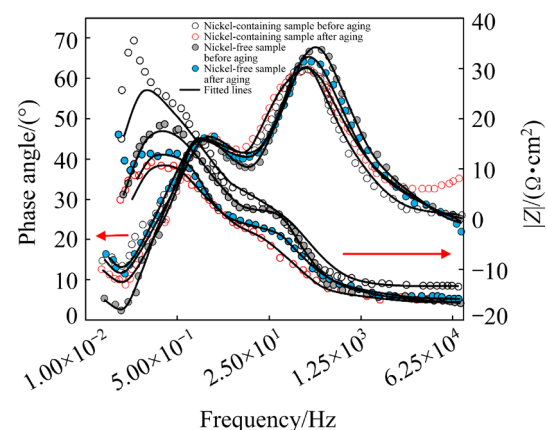**Fig. 8** Nyquist diagrams of nickel-containing and nickel-free samples

Fig. 9 Bode plots of nickel-containing and nickel-free samples

Table 1 Electrochemical parameters of different samples

Sample	φ_{corr} (vs SCE)/V	J_{corr}/ (A·cm^{-2})	R_{pol}/ (kΩ·cm^2)	R_{corr}/ (kΩ·cm^2)
Nickel-containing before aging	−1.02	3.21×10^{-5}	31.74	33.24
Nickel-containing after aging	−1.33	1.89×10^{-4}	7.11	9.34
Nickel-free before aging	−1.09	5.11×10^{-5}	21.38	24.12
Nickel-free after aging	−1.27	1.09×10^{-4}	11.69	13.56

−1.09 V (vs SCE) was obtained before aging heat treatment and reduced to a lower value of −1.27 V (vs SCE) after aging heat treatment. Corrosion potential of −1.02 and −1.33 V (vs SCE) was obtained in the sample containing nickel before and after aging heat treatment, respectively. Meanwhile, the pitting potential of −0.55 and −0.78 V (vs SCE) in nickel-free samples was obtained before and after heat treatment, respectively. However, the pitting potential of −0.51 and −0.77 V (vs SCE) in the sample containing nickel was obtained before and after heat treatment, respectively. This indicated that before heat treatment, the passive films of samples containing nickel-aluminide could survive at a higher potential than those without nickel one. Moreover, the corrosion current density (J_{corr}) was approximated using the Stern−Geary equation, and the polarization resistance (R_{pol}) was obtained from the linear region [23].

Before aging heat treatment, nickel-containing coatings showed a lower corrosion current density than nickel-free coatings, indicating that nickel-containing coatings had a lower corrosion rate. Heat treatment on the coatings increased the corrosion current density in nickel-containing and nickel-free coatings. The pitting corrosion is mainly attributed to the potential difference between the matrix and precipitates and under the influence of a wide range of microstructural features, including the size and spaces between precipitates, precipitate-free zones, and the concentration gradient of soluble elements [24]. Nickel-containing particles act as insulators, preventing galvanic coupling between the substrate and precipitates and improving pitting corrosion resistance. The presence of nickel-containing particles significantly improves the pitting corrosion resistance. Limited studies have

been performed on the effect of nickel on the corrosion behavior of the aluminum alloy. It has been observed that the homogeneous distribution of nickel-aluminide improves the corrosion resistance of aluminum alloy [25]; however, the non-uniform distribution reduces the corrosion resistance of aluminum alloy [26]. It should be noted that the presence of finer precipitates after heat treatment in both nickel-containing and nickel-free samples can improve the pitting corrosion resistance. The effect of heat treatment and the presence of nickel-rich particles caused a complex corrosion behavior in the nickel-containing sample. Before aging heat treatment, in the nickel-containing sample, although some copper absorbed by nickel-containing particles and particles nobler than the matrix formed, reducing the amount of soluble copper in the aluminum matrix can increase the potential difference between the particle and the matrix. Therefore, this phenomenon has a detrimental effect on corrosion behavior. Measurement of the amount of copper in the aluminum matrix of nickel-containing samples before heat treatment showed that the content of soluble copper in the aluminum matrix is higher than that after the heat treatment, which is 0.35 and 0.29 at.%, respectively. In the nickel-free sample, due to the higher friction surfacing process temperature, the precipitates become coarser and as a result, the amount of soluble copper in the aluminum matrix decreases. Under these conditions, the corrosion sensitivity in the nickel-free sample increases due to the increase in the potential difference between the precipitates and the substrate.

Corrosion resistance decreases after aging due to the reduced soluble copper in the nickel-containing sample and the adsorption of more significant amount of soluble copper by nickel-rich particles. The content of soluble copper in the aluminum matrix in the sample with and without nickel after heat treatment is 0.12 and 0.18 at.%, respectively. On the other hand, it should be noted that after aging heat treatment, the sample without nickel has shown higher corrosion resistance than the sample containing nickel. Due to the formation of fine precipitates distributed throughout the microstructure and the reduction of the surface subjected to corrosion, the corrosion of nickel-free sample is reduced compared to this sample before the aging heat treatment. The lower corrosion

resistance with the increasing size of precipitates has also been reported in Refs. [27,28]. For Cu-containing Al−Zn−Mg alloy, Cu incorporates in the clusters, GP zones, η, and η' precipitates [29]. Based on the work of SHA and CEREZO [30], the matrix Cu content from the under-aged to peak-aged tempers decreased very slowly, indicating that the corresponding Cu content in η precipitates increased extremely slowly. Therefore, it can be expected that the aging heat treatment in the sample without nickel will not have great effect on the amount of soluble copper in the aluminum matrix. The EIS data were fitted with the appropriate equivalent circuit for further insight into the corrosion behavior. Based on Ref. [31], a model can be presented according to Fig. 10. Excellent agreement between the fitted and experimental EIS data was obtained. In this model, R_{sl}, R_o, and R_{pol} were the solution resistance, the passive film resistance, and polarization resistance, respectively. The C_o and C_{dl} are capacitances of the passive film and electrical double layer, respectively. According to the proposed model, the equivalent corrosion resistance (R_{corr}) of different samples is presented in Table 1. As is evident, the model results also confirm the higher corrosion resistance of the sample containing nickel-aluminide before heat treatment and lower corrosion resistance after heat treatment.
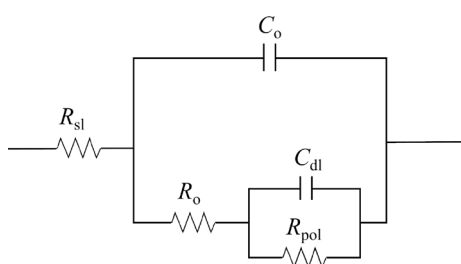

Fig. 10 Model used to investigate corrosion behavior

4 Conclusions

(1) The dissolution of reinforcing precipitates during solid solution treatment and the absence of secondary phase particles result in significant grain growth in the nickel-free sample.

(2) The presence of nickel-rich particles causes the adsorption of copper in the aluminum matrix, leading to a reduction of soluble copper in the aluminum matrix. After solid solution and aging

heat treatment of sample containing nickel, due to providing more opportunity to absorb copper in the aluminum matrix, the possibility of S-Al$_2$CuMg precipitates during aging decreases.

(3) Before aging heat treatment, the pitting corrosion resistance is significantly improved by the presence of nickel-containing particles. In the nickel-free sample, before the aging heat treatment, the corrosion sensitivity in the nickel-free sample increases due to the increase in the potential difference between the precipitates and the substrate. After aging heat treatment, the sample without nickel has shown 64.4 % more corrosion resistance than the sample containing nickel.

References

[1] XIA D H, PAN C C, QIN Z B, FAN B M, SONG S Z, JIN W X, HU W B. Covalent surface modification of LY12 aluminum alloy surface by self-assembly dodecyl phosphate film towards corrosion protection [J]. Progress in Organic Coatings, 2020, 143: 105638.

[2] PAN C C, WANG X Z, BEHNAMIAN Y, WU Z B, QIN Z, XIA D H, HU W B. Monododecyl phosphate film on LY12 aluminum alloy: pH-controlled self-assembly and corrosion resistance [J]. Journal of the Electrochemical Society, 2020, 167(16): 161510.

[3] WANG W C, LI J X, GE Y, KONG D J. Structural characteristics and high-temperature tribological behaviors of laser cladded NiCoCrAlY−B$_4$C composite coatings on Ti$_6$Al$_4$V alloy [J]. Transactions of Nonferrous Metals Society of China, 2021, 31(9): 2729−2739.

[4] ZENG M, YAN H, YU B B, HU Z. Microstructure, microhardness and corrosion resistance of laser cladding Ni−WC coating on AlSi$_5$Cu$_1$Mg alloy [J]. Transactions of Nonferrous Metals Society of China, 2021, 31(9): 2716−2728.

[5] YOUSEFI E, SHARAFI S, IRANNEJAD A. Microstructure, tribological behavior and magnetic properties of Fe−Ni−TiO$_2$ composite coatings synthesized via pulse frequency variation [J]. Transactions of Nonferrous Metals Society of China, 2021, 31(12): 3800−3813.

[6] ZOU K, ZOU J P, DENG C M, LIU M, LIU X Z, ZHAO R M, LI S H, ZHU R B, GAO D. Preparation and properties of supersonic atmospheric plasma sprayed TiB$_2$−SiC coating [J]. Transactions of Nonferrous Metals Society of China, 2021, 31(1): 243−254.

[7] RAJARAM G, KUMARAN S, RAO T S. Effect of graphite and transition elements (Cu, Ni) on high temperature tensile behaviour of Al−Si alloys [J]. Materials Chemistry and Physics, 2011, 128(1/2): 62−69.

[8] LATTANZI L, DI GIOVANNI M T, GIOVAGNOLI M, FORTINI A, MERLIN M, CASARI D, DI SABATINO M, CERRI E, GARAGNANI G. Room temperature mechanical

properties of A356 alloy with Ni additions from 0.5 wt.% to 2 wt.% [J]. Metals, 2018, 8(4): 224.

[9] ASGHAR Z, REQUENA G, KUBEL F. The role of Ni and Fe aluminides on the elevated temperature strength of an AlSi$_{12}$ alloy [J]. Materials Science and Engineering A, 2010, 527(21/22): 5691−5698.

[10] NAEEM H T, MOHAMMED K S, AHMAD K R, RAHMAT A. The influence of nickel and tin additives on the microstructural and mechanical properties of Al−Zn−Mg−Cu alloys [J]. Advances in Materials Science and Engineering, 2014, 2014: 1−10.

[11] AKOPYAN T K, PADALKO A G, BELOV N A, KARPOVA Z A. Effect of barothermal treatment on the structure and the mechanical properties of a high-strength eutectic Al−Zn−Mg−Cu−Ni aluminum alloy [J]. Russian Metallurgy, 2017, 2017(11): 922−927.

[12] SURESH S, GOWD G H, DEVA KUMAR M. Experimental investigation on mechanical properties of Al 7075/Al$_2$O$_3$/Mg NMMC's by stir casting method [J]. Sādhanā, 2019, 44(2): 51.

[13] KHAKI-DAVOUDI S, NOUROUZI S, JAMSHIDI AVAL H. Microstructure and mechanical properties of AA7075/Al$_3$Ni composites produced by compocasting [J]. Materials Today Communications, 2021, 28: 102537.

[14] SALARIEH S, NOUROUZI S, JAMSHIDI AVAL H. An investigation on the microstructure and mechanical properties of Al−Zn−Mg−Cu/Ti composite produced by compocasting [J]. International Journal of Metalcasting, 2022, 16: 1397−1414.

[15] FARKOOSH A R, JAVIDANI M, HOSEINI M, LAROUCHE D, PEKGULERYUZ M. Phase formation in as-solidified and heat-treated Al−Si−Cu−Mg−Ni alloys: Thermodynamic assessment and experimental investigation for alloy design [J]. Journal of Alloys and Compounds, 2013, 551: 596−606.

[16] MONDOLFO L F. Aluminum alloys: Structure and properties [M]. Amsterdam: Elsevier, 2013.

[17] MA K, WEN H, HU T, TOPPING T D, ISHEIM D, SEIDMAN D N, LAVERNIA E, SCHOENUNG J. Mechanical behavior and strengthening mechanisms in ultrafine grain precipitation-strengthened aluminum alloy [J]. Acta Materialia, 2014, 62: 141−155.

[18] GAZIZOV M, KAIBYSHEV R. Precipitation structure and strengthening mechanisms in an Al−Cu−Mg−Ag alloy [J]. Materials Science and Engineering A, 2017, 702: 29−40.

[19] RYEN Ø, HOLMEDAL B, NIJS O, NES E, SJÖLANDER E, EKSTRÖM H E. Strengthening mechanisms in solid solution aluminum alloys [J]. Metallurgical and Materials

Transactions A, 2006, 37(6): 1999−2006.

[20] STARINK M J, WANG S C. A model for the yield strength of overaged Al−Zn−Mg−Cu alloys [J]. Acta Materialia, 2003, 51(17): 5131−5150.

[21] LEE S H, JUNG J G, BAIK S I, SEIDMAN D N, KIM M S, LEE Y K, EUH K. Precipitation strengthening in naturally aged Al−Zn−Mg−Cu alloy [J]. Materials Science and Engineering A, 2021, 803: 140719.

[22] LIU F, ZHU X, JI S. Effects of Ni on the microstructure, hot tear and mechanical properties of Al−Zn−Mg−Cu alloys under as-cast condition [J]. Journal of Alloys and Compounds, 2020, 821: 153458.

[23] VISSER P, TERRYN H, MOL J M C. On the importance of irreversibility of corrosion inhibitors for active coating protection of AA2024-T3 [J]. Corrosion Science, 2018, 140: 272−285.

[24] JI Y Y, XU Y Z, ZHANG B B, BEHNAMIAN Y, XIA D H, HU W B. Review of micro-scale and atomic-scale corrosion mechanisms of second phases in aluminum alloys [J]. Transactions of Nonferrous Metals Society of China, 2021, 31(11): 3205−3227.

[25] MOHAMMED A, YARO S, ABDULWAHAB M. Influence of Ni additions and age-hardening treatment on the corrosion resistance of Al−Cu−Si alloy [J]. Journal of Materials and Environmental Science, 2016, 7(5): 1549−1555.

[26] VISHWANATHA A D, PANDA B, SHIVANNA D M. Effect of a T6 aging treatment on the corrosion behaviour of in-situ Al$_x$Ni$_y$ reinforced AA6061 composite [J]. Materials Today: Proceedings, 2021, 44: 4112−4117.

[27] SON I J, NAKANO H, OUE S, KOBAYASHI S, FUKUSHIMA H, HORITA Z. Pitting corrosion resistance of anodized aluminum−copper alloy processed by severe plastic deformation [J]. Materials Transactions, 2008, 49(11): 2648−2655.

[28] RALSTON K, BIRBILIS N. Effect of grain size on corrosion: A review [J]. Corrosion, 2010, 66(7): 075005−075013.

[29] WANG S S, HUANG I W, YANG L, JIANG J T, CHEN J F, DAI S L, SEIDMAN D N, FRANKEL G, ZHEN L. Effect of Cu content and aging conditions on pitting corrosion damage of 7xxx series aluminum alloys [J]. Journal of the Electrochemical Society, 2015, 162(4): C150.

[30] SHA G, CEREZO A. Early-stage precipitation in Al−Zn−Mg−Cu alloy (7050) [J]. Acta Materialia, 2004, 52(15): 4503−4516.

[31] YU M, ZHAO H, ZHANG Z, ZHOU L, SONG X, MA N. Texture evolution and corrosion behavior of the AA6061 coating deposited by friction surfacing [J]. Journal of Materials Processing Technology, 2021, 291: 117005.

时效热处理对摩擦堆焊
铝基复合材料显微组织和腐蚀行为的影响

Hamed JAMSHIDI AVAL

Department of Materials Engineering, Babol Noshirvani University of Technology,
Shariati Avenue 47148-71167, Babol, Iran

摘　要：研究人工时效热处理对 Al−Zn−Mg−Cu 基复合材料显微组织和腐蚀行为的影响。采用搅拌铸造工艺原位制备铝化镍增强 Al−Zn−Mg−Cu 合金复合材料，采用摩擦堆焊法将该铸态复合材料耗材杆堆焊在 AA1050 铝合金基体上，并在 125 ℃进行人工时效热处理 18 h。结果发现，无镍合金中晶粒发生明显长大。此外，复合材料显微组织中铝化镍增强相的存在导致双态组织的形成。富镍颗粒的存在和析出相的强化机制使含镍材料的硬度和强度得到提高。经人工时效热处理后，含铝化镍复合材料的剪切强度和硬度比铝基体分别提高了 24%和 13%。含镍颗粒的存在显著提高了未热处理合金的耐点蚀性能。经时效热处理后，含镍样品的耐腐蚀性比不含镍样品降低了 39%，这是因为含镍样品中的富镍颗粒吸附了更多的可溶性铜。
关键词：铝基复合材料；铝化镍增强相；摩擦堆焊；人工时效热处理；腐蚀行为

(Edited by Wei-ping CHEN)